Progress In Electromagnetics Research C, Vol. 70, 111–122, 2016

MIMO Propagation Measurements in Underground Mine Using Beamforming Butler Matrix Networks

Mohamad Ghaddar[1], Mourad Nedil[1, *], Larbi Talbi[2], and Ismail Ben Mabrouk[2]

Abstract—The advantages of integrating beamforming Butler matrix in 4×4 Multiple-Input Multiple-Output (MIMO) systems for underground mine wireless communications in the 2.4 GHz band are investigated. To satisfy both line-of-sight (LOS) and non-line-of-sight (NLOS) conditions, two separate measurement campaigns are performed in a real L-shaped underground mine gallery; the first uses 4-elements beamforming conformal microstrip patch arrays (CMPA), while the second uses 4-elements beamforming Butler Network (BN-MIMO) by means of connecting a planar microstrip patch array to a Butler matrix. Due to its high radiation efficiency, the latter shows further performance for enhancing the channel propagation characteristics, and thus, for reducing the average path loss by about (2.2 dB, 5.1 dB) under (LOS, NLOS) conditions, respectively. Similarly, a reduction of (0.67 ns, 37 ns) in the RMS delay spread has been achieved to result in an additional gain of (46 MHz, 0.82 MHz) in the channel's coherence bandwidth. Furthermore, the orthogonal property of BN array radiation beams has led to a suppression of about (6%, 11%) in inter-subchannels correlations to boost (1.1 bit/s/Hz, 4.35 bit/s/Hz) in the channel capacity.

1. INTRODUCTION

Recently, the mining industry has expressed more interest towards the adoption of reliable wireless communications systems aiming to optimize both the mining processes and the miners' safety [1]. Technically, the achievement of such a goal faces significant challenges as a consequence of the hostile propagation characteristics of underground mines environments [2, 3]. Indeed, MIMO technology that sufficiently exploits both the abundant multipath and frequency resources offers a great potential for high data throughput speed as it allows spatial multiplexing, diversity, and beamforming schemes [4].

In underground mines, a recent study has been carried out to investigate the performance of MIMO Beam-Space (BS) system based on a switched beam conformal array antenna (CMPA) [5]. Such a shiftless structure shows several drawbacks as it limits the orientation of its radiation beams towards 30° angles facing the array, exclusively. Furthermore, the static beams orientation of CMPA was a major concern while technical requirements for smart detection of channel multipath at desirable angles of arrival (AoA) were ignored. Although underground mine wireless channels are subject to hostile propagation phenomenon which leads to large multipath fading fluctuations, such effects decrease the spectral efficiency of the system and limit its capacity. Thus, CMPA might become irrelevant under an insufficient link power budget. Fortunately, Butler matrices act as electronic steerable passive radiators, and they allow the orientation of the radiation directivity towards the desired angles using electronic phase shifters [6]. Alternatively, due to their simple implementation, high radiation efficiency and non-physical beam steering, Butler matrices become widely employed in the multi-beam arrays industry [7]. Such radiators can be configured as MIMO system with M-elements that transmit/receive

Received 21 June 2016, Accepted 3 November 2016, Scheduled 4 January 2017

* Corresponding author: Mourad Nedil (mourad.nedil@uqat.ca).

[1] School of Engineering, University of Quebec (UQAT), Val d'Or, Quebec, Canada. [2] Department of Computer Science and Engineering, University of Quebec (UQO), Gatineau, Quebec, Canada.

simultaneously [8]. Recent studies have confirmed the integration of Butler matrix in MIMO systems for enhancing the multipath gains and mitigating the fading correlation among array elements [9].

Unlike CMPA, the proposed smart beamforming system shows a potential ability to gather the array's orthogonal and uncorrelated sub-beams to result in a high gain beamforming lobe at each port of the array, instantaneously. Thus, BN-MIMO radiation setup ensures an efficient directional radiation beam that can be shifted instantly towards desired angles to strengthen the multipath gain in these directions. Besides, the directivity of such a technique limits the multipath interference and thus enhances the channel spectral efficiency.

To the best of our literary search, the advantages of using Butler matrix-MIMO systems in underground mines have not been explored yet. To give a clear insight into the proposed system, the extracted results will be fairly referred to a previous work reported in [5] which is performed under a similar measurement setup and procedure in the considered gallery site. Thus two separate 4×4 MIMO measurement campaigns are performed in a real underground mine using: a) 4-elements beamforming Conformal Microstrip Patch Arrays (CMPA), and then b) 4-elements beamforming Butler Network (BN) by means of a linear planar microstrip patch array connected to a Butler matrix. For analysis purpose, both campaigns are investigated in a comparative way, under both LOS and NLOS scenarios, hence, an L-shaped mine gallery is chosen. Regardless of the undertaken scenarios, the achieved results have confirmed the use of BN array as a means to enhance the propagation characteristics, and thus, to boost MIMO system capacity of underground mines channels.

The rest of the paper is organized as follows. Section 2 introduces the channel sounder hardware setup and describes the measurement site and procedure. The statistical analysis of the experimental data and results are presented in Section 3, and followed by a conclusion in Section 4.

2. MEASUREMENTS SETUP, SITE AND PROCEDURE

The frequency-sweep measurements are performed using the sounder setup detailed in [5]. The measurement setup parameters are summarized in Table 1. Both arrays are designed and fabricated in the LRTCS (Laboratoire de recherche Télébec en communications souterraines) using HFSS software tool (Ansoft). Fig. 1 shows a photograph of the used CMPA array, and its full details are provided in [5].

Table 1. Measurement system parameters.

Parameters	Values
Center frequency	2.45 GHz
Bandwidth	200 MHz
Number of Frequency Tones	4001
Frequency Resolution	50 KHz
Time resolution	5 ns
Transmit Power	10 dBm
Low Noise Amplifier (LNA)	30 dB
Power Amplifier (PA)	30 dB
Dynamic Range	100 dB

2.1. Butler Network Design and Structure

BN offers a potential ability to be equipped by a sophisticated RF switch which facilitates the radiation beam steering of the arrays. This technique is an attractive option for complex underground mine channels due to its simple design, lossless property, high beam crossover level and ability of forming orthogonal beams. Full details about Butler matrix technology are provided in [6]. Practically, a switched-beam BN consists of a fixed beamforming network and a planar microstrip patch antenna array as shown in Fig. 2(a). The Butler matrix is composed of 3-dB branch line couplers, a cross-over,

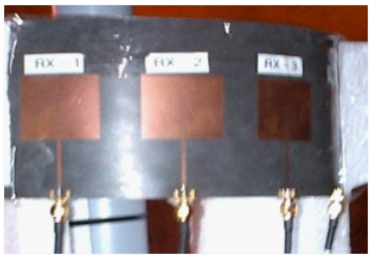

Figure 1. A photograph of Beamforming conformal microstrip patch array (CMPA) detailed in [5].

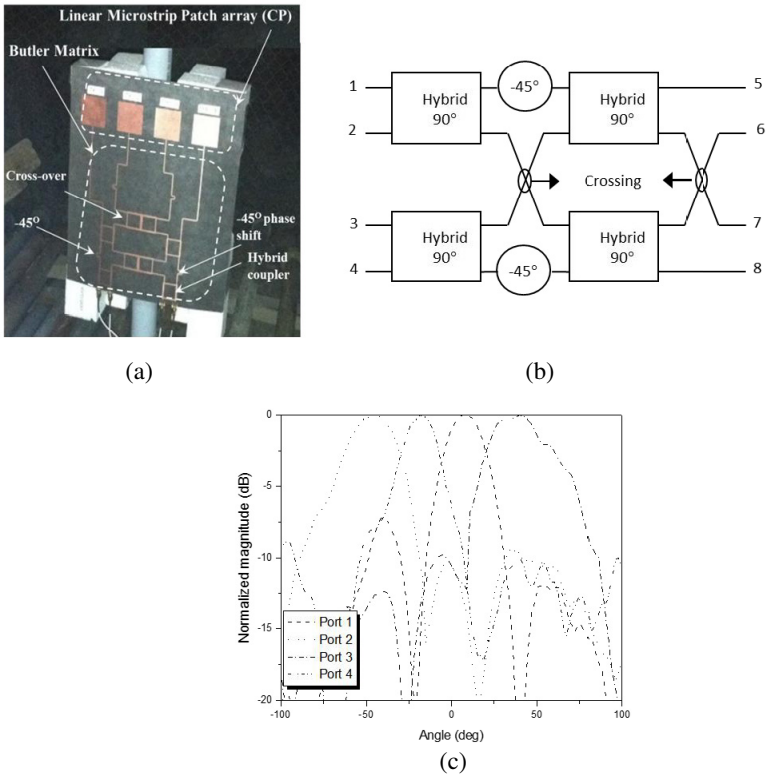

Figure 2. (a) A photograph, (b) a design block diagram and (c) the measured H-plane radiation patterns of the fabricated Butler network array (BN).

and transmission line phase shifters [6]. The trend towards such a design is to tool-up the linear planar array with the necessary phase shift that produces multiple orthogonal beams. A block diagram of the Butler matrix is shown in Fig. 2(b). The radiation pattern performance in the H-plane was measured in an anechoic chamber as shown in Fig. 2(c). Similar to CMPA array, BN provides four beams at $-45°$, $-15°$, $15°$ and $45°$. However, the BN shows a competitive advantage over CMPA due to its higher level of beams radiation directivity which plays an important role in mitigating multipath fading effects and in enhancing the channel propagation characteristics. To ensure almost uncorrelated subchannels, the array elements are spaced by one-half wavelength ($\lambda/2$) [1]. Although increasing the number of array elements is expected to enhance the channel performance, the available designed arrays are limited to four elements. Such a choice appears persuasive under IEEE 802.11n standard specifications that allows up to four spatial streams.

An illustrative map and a photograph of the measurement site gallery are shown in Fig. 3. More description details about its structure are provided in [5]. Such a persuasive choice of the measurement site ensures a reasonable referral of the achieved results to the literature. The undertaken hostile-

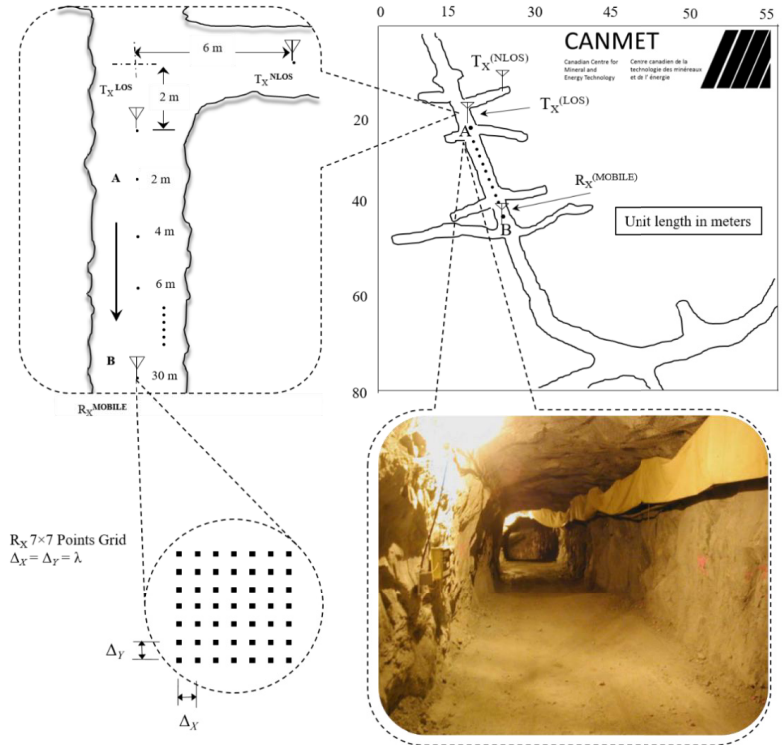

Figure 3. Illustrative map of the CANMET 40 m level underground mine gallery in Val d'Or, Quebec, Canada, and of the T_X/R_X arrays positions.

propagation mine gallery suffers from a significant amount of multipath as a result of reflection, diffraction as well as scattering mechanisms from the surrounding rough surfaces. During measurements, each scenario was performed using two identical T_X/R_X arrays, i.e., either CMPA or BN. Similar to the procedure detailed in [5], the small scale measurements were obtained by arranging R_X on a 7×7 points square grid spaced by $\lambda/2$. LOS and NLOS scenarios were investigated as illustrated in Fig. 3. a) *LOS scenario*: T_X remains stationary at the intersection of the gallery passageways while Rx is moving away from point "A" to point "B" (2 to 30 m), with an increment of 2 m. b) *NLOS scenario*: This measurement campaign is similar to the previous one. The initial position of R_X is set at point "A" (Fig. 3) to guarantee LOS blockage between both ends, and then R_X moves towards its final position (point B) with an increment of 2 m. Following the procedure in [5], the 3-D MIMO channel matrix at each R_X location is formed by collating CTFs of all $(4 \times 4 = 16)$ subchannels, where N_R, N_T are the number of transmit, receive array elements, and f is the discrete frequency component (4001).

3. EXPERIMENTAL ANALYSIS AND RESULTS

The extracted results will be fairly referred to the measurements reported in [5] as they were performed in the undertaken mine gallery using similar procedure, setup and CMPA arrays. The channel multipath effects are examined after eliminating the sounding system hardware including the transmit power, arrays gains and feeding cables losses. This is realized by calibrating (normalization) all measured complex Channel Transfer Functions (CTF) with respect to 1 m of TX-RX distance [5].

3.1. Link Budget and Fading Characterization

3.1.1. Distance-Dependent Path Loss (PL) Law

The measured PL has been examined prior to other statistical parameters as it relates the received power (P^r) to the transmitted power (P^t) for each MIMO subchannel and for each T_X-R_X separation distance

(d). We stress that averaging of the channel transfer function (H) measured across 4001 frequency tones (2.35–2.55 GHz) was done on a linear scale (not in decibels) as:

$$P^r_{\mathrm{dB}}(d) = 10\log_{10}\left\{\left(\frac{1}{400}\right)\sum_{i=1}^{4001}|H(f_i,d)|^2\right\} - [P^r_{\mathrm{dBm}} w.r.t. 1\,\mathrm{m}] \tag{1}$$

Thus, the location-variant PL is extracted as [11]:

$$\overline{PL}_{\mathrm{dB}}(d) = \overline{PL^r_{\mathrm{dB}}}(d_o) + 10n\log_{10}\left(\frac{d}{d_o}\right) + S_{\mathrm{dB}} \tag{2}$$

where $\overline{PL^r_{\mathrm{dB}}}(d_o)$ is the averaged received power in decibels at a reference distance d_o from T_X, in our case $d_o = 1\,\mathrm{m}$; "n" is the PL exponent; S_{dB} denotes the location-dependent shadowing fading parameter. Scatter plots of PL averaged over all MIMO subchannels versus T_X-R_X logarithmic distances and the Minimized Mean Squared Error (MMSE) fitting lines are presented in Fig. 4. The fluctuation in PL around its mean is the result of the significant variations in the dominant waves with respect to the sum of heavy multipath in the channel. Indeed, underground mines structures are location-specific, i.e., their non-uniform cross section leads to a noticeable variation in the amount of multipath from one location to another [12]. Table 2 shows the average PL, "n" and S_{dB} of Eq. (2).

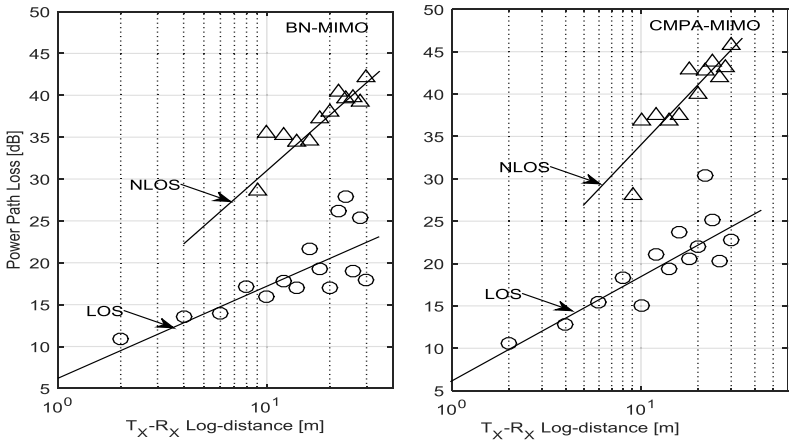

Figure 4. Channel path loss (PL) measured using (a) BN-MIMO and (b) CMPA-MIMO in [5].

Table 2. Average Path Loss (PL), Path Loss Exponent (n), Standard Deviation (S_{dB}), Average SNR and Ricean K_{Factor}.

Array Type:	CMPA-MIMO		BN-MIMO	
Scenario:	LOS	NLOS	LOS	NLOS
n	1.18	2.56	1.13	2.24
PL [dB]	18.45	38.7	1623	33.2
S_{dB} [dB]	3.61	2.65	3.73	3.1
SNR [dB]	37.2	15.7	41.4	19.3
K_{Factor} [dB]	6.1 (Rice)	−1.63 (Rayleigh)	7.7	1.2

Under LOS, the value ($n \leq 2$) implies that underground mine signals exhibit a higher propagation ability than free space. In fact, underground mine tunnels act as waveguides for propagating signals where all multipath rays aggregate and contribute to enhancing the received power [13]. "n" of both MIMO configurations exhibit a very slight difference of about 0.9 and 0.32 in favor of BN for LOS and

NLOS cases, respectively. Despite this slight difference in "n", however, BN-MIMO offers a noticeable suppression in the average PL of about 2.2 dB and 5.13 dB for LOS and NLOS cases, respectively. As compared to LOS case, a larger PL gap is noticed under NLOS, owing to the heavy amount of multipath experienced using BN-MIMO compared to CMPA-MIMO thus confirming the importance of the high radiation directivity of BN array for enhancing the multipath gains in the channel. The large values of S_{dB} reflect the variation in the received power with respect to its mean.

3.1.2. Signal-to-Noise Ratios (SNR)

Given the channel setup information, *SNRs* (in dB) of all $N_T \times N_R$ subchannels are calculated as a function of T_X-R_X distance along the galley as:

$$\mathrm{SNR}(d) = \underbrace{P_T + G_T + G_R - \overline{PL}_{\mathrm{dB}}(d)}_{\textit{Received Power Sensitivity}} - NP \tag{3}$$

where, the transmitted power, gains G_T, G_R of T_X, R_X antennas, respectively, are assumed 0 dB, and the receiver noise power (NP) is -90 dBm. The feeding cables losses are compensated by the power amplifier (PA) and low noise amplifier (LNA) of the system, hence, they are considered to be 0 dB. The empirical CDF of the channel's SNR is shown in Fig. 5(a). The computed average *SNR* is given in Table 2. Fig. 5(a) gives a discernment into the BN-MIMO radiation effects; theoretically, a coherent combination of $N_T \times N_R$ copies of the transmitted signal superimposed by a large amount of strong channel multipath results in a higher received power level and in a further suppression in the noise power. BN arrays show a higher ability to generate strong multipath in the channel, and indeed, greater SNRs are achieved than CMPA case.

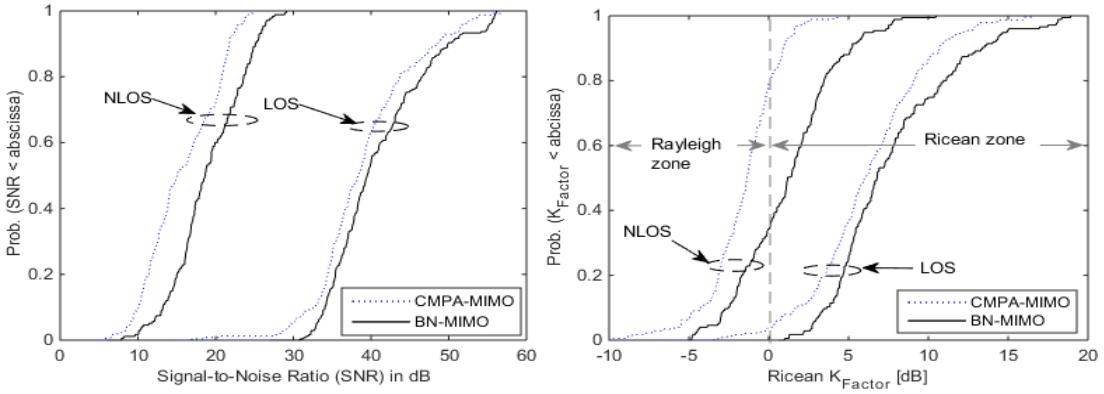

Figure 5. Cumulative distribution function (CDF) of (a) Signal-to-Noise Ratio (SNR), (b) *Ricean* K_{Factor}.

3.1.3. Ricean K-Factor

In the literature, Ricean K_{Factor} is used extensively to characterize the fading in multipath channels, i.e., a large K_{Factor} gives an indication about the presence of shallow fades, while the worst-case, i.e., Rayleigh, assumes the absence of any dominant multipath in the channel. Thus, a LOS channel is commonly assumed for Ricean fading, but there can be dominant components in NLOS scenarios. For a 3-D MIMO matrix $\mathbf{H}$ containing the frequency-dependent observations of the subchannel responses, K_{Factor} is computed for each individual MIMO subchannel and for each R_X location throughout the gallery [14]:

$$K_{Factor} = 10\log_{10}\left\{\frac{\varepsilon(|\mathbf{H}|)^2}{2var(|\mathbf{H}|)}\right\} \tag{4}$$

where $\varepsilon\{\}$ and $var\{\}$ correspond to the expectation and variance operators, respectively. Results of Fig. 5(b) and Table 2 demonstrate that the multipath fadings of BN-MIMO are Ricean distributed. The value of Ricean K_{Factor} that varies between 7.7 dB and 1.2 dB for LOS and NLOS, respectively, demonstrates the presence of strong dominant multipath in BN-MIMO channel. Under NLOS, BN-MIMO exhibits less severe fading level than Rayleighan CMPA-MIMO.

3.2. Time Dispersive Channel Characteristics

3.2.1. Power Delay Profile (PDP)

Since the measurements are performed using the frequency-sweep technique, the channel PDP is obtained by applying the inverse discrete Fourier transform (IDFT) to the complex MIMO CTF measured at each R_X location (d).

$$\mathrm{PDP}^{N_R\times N_T}(t,d) = \left\langle \left| IDFT\left\{H^{N_R\times N_T}(f,d)\right\}\right|^2 \right\rangle \tag{5}$$

The PDP is then averaged over 16 subchannels measured at each of the 15 R_X locations along the central line of the gallery (10 locations in NLOS case). In Fig. 6(a), the first perceptible paths dominating the PDP are the result of the direct LOS waves for each R_X location; their delays range from 6.7 ns to 100 ns for 2 m to 30 m which corresponds to the shortest T_X-R_X path distances, respectively. As observed, the magnitude of the LOS along the gallery does not decrease in a monotonic trend as experienced in indoor environments; it fluctuates at some specific distances. Such manifestation might be due to the location-specific nature of underground mines as their cross sectional shapes are not uniform, and their surfaces irregularities can vary up to 30 cm. Indeed, the mean of the signal power fluctuates randomly throughout the location-specific gallery and thus gives rise to the log-normally shadow fading phenomenon [15]. Such manifestation is obvious in Fig. 4 as the calculated PL for all Rx locations deviate randomly from their regression fitting lines. Fig. 6(b) presents two NLOS-PDPs samples measured at 30 m from R_X using both CMPA-MIMO and BN-MIMO setups. The latter shows an exponentially decaying PDP of strong multipath where the peak power of the PDP reaches about 50 dB above the noise level compared to about 30 dB under CMPA-MIMO.

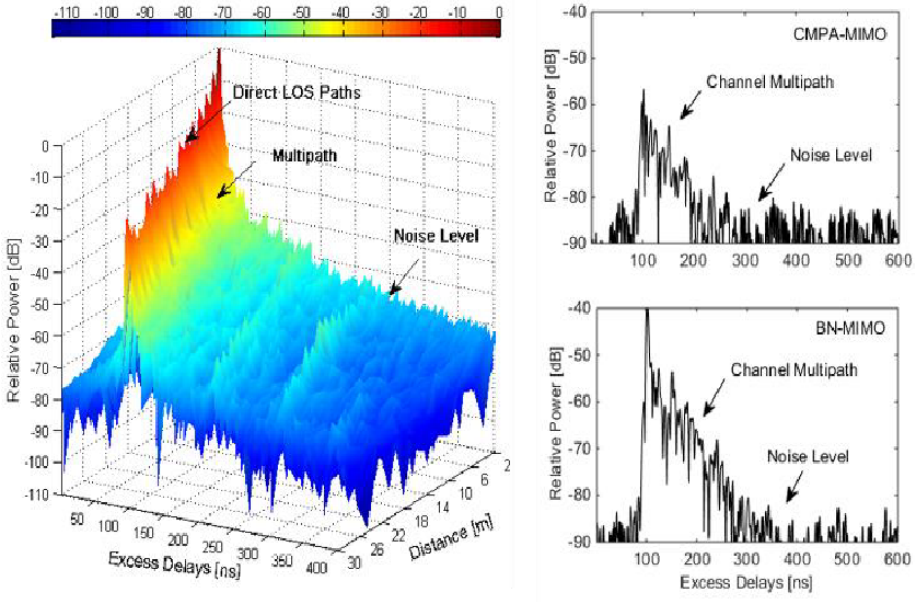

(a) (b)

Figure 6. Channel time dispersion characteristics (a) BN-MIMO normalized PDP measured under LOS for all R_X locations, (b) PDP samples measured under NLOS at 30 m from R_X.

3.2.2. Root Mean Square Delay (σ_t) and Coherence Bandwidth (B_C)

RMS delay spread (σ_t) gives insight into the channel dispersive characteristics, the coherence bandwidth and thus, the amount of inter-symbol interference (ISI) to be encountered in the channel. It is extracted from the channel PDP as [5]

$$\sigma_t = \sqrt{\frac{\Sigma_k \alpha_k^2 \tau_k^2}{\Sigma_k \alpha_k^2} - \left(\frac{\Sigma_k \alpha_k^2 \tau_k}{\Sigma_k \alpha_k^2}\right)^2} \tag{6}$$

where α_k and τ_k are the relative magnitude and delay of each perceptible multipath component, respectively. σ_t are extracted from the corresponding PDP using the threshold level considered in [5] that is 10 dB below 0 dB peak of the normalized PDP, thus σ_t will be fairly referred to those obtained in [5]. During data analysis, σ_t was found to increase with T_X-R_X distances, but not in a monotonic trend due to the aforesaid site-specific reasons of the gallery. However, regardless of the traveled distance and the great amount of multipath experienced in underground mines, smaller σ_t values have been frequently recorded than those obtained in indoor environments where the average σ_t reaches 15.94 ns and 24.72 ns for LOS and NLOS cases, respectively [16]. Owing to the waveguiding effects of confined underground mines, at large distances the reflected, diffracted and scattered copies of the travelling signal arrive at R_X with relatively small delays as compared to the direct LOS path [17]. Fig. 7 shows CDF of σ_t computed for all ($N_R \times N_T$) MIMO subchannels and for all Rx locations throughout the gallery. The mean value is computed by averaging σ_t over the 16 subchannels and R_X locations throughout the gallery ($16 \times 15 = 240$ for LOS case) as summarized in Table 3. Regardless of the undertaken scenario and T_X-R_X locations, BN-MIMO demonstrates lower σ_t than the values reported in [5]. Further reductions in the average values of σ_t are achieved at a rate of 0.67 ns, 37 ns for LOS and NLOS cases, respectively. Thus, the presented BN array offers considerably short σ_t implying lower design complexities for the equalization tools required to counter the erroneous bits in the channel [18]. Furthermore, the channel coherence bandwidth (B_C) is computed [15]. As expected, during the data processing, it is found that shorter communication links offer more useful B_C. Under BN-MIMO, additional B_C of 4.6 MHz and 0.82 MHz have been achieved for LOS and NLOS cases, respectively, as compared to CMPA-MIMO. The

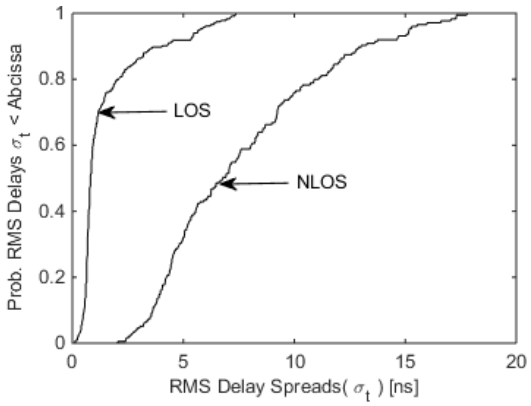

Figure 7. Cumulative distribution function (CDF) of the RMS delays Spreads measured using BN-MIMO.

Table 3. Statistics of RMS delays and average coherence bandwidth [MHz].

Array Type:		CMPA [5]		BN-MIMO	
Scenario:		LOS	NLOS	LOS	NLOS
σ_t [ns]	mean	2.08	11.47	1.41	7.8
	std.	1.16	4.7	0.96	3.93
B_C [MHz]	mean	9.61	1.74	14.2	2.56

latter requires therefore more equalization measures for an equivalent spectral efficiency. The statistics of B_C are listed in Table 3.

3.3. Inter-Subchannels Correlation Coefficients

The correlation coefficients give useful information about MIMO inter-subchannels orthogonality and thus about the capacity performance. In other words, a higher capacity can be reached when different transmission channels carry independent uncorrelated copies of the transmitted signal. The correlation of the channel gains from the same transmitter to four different receivers (receiver correlation) is calculated first and then, the correlation of the channel gains from four different transmitters to the same receiver (transmitter correlation) [19]. The correlation coefficients (ρ) of channel gains for two different receive antenna elements (n_1 and n_2) and the correlation coefficients for two different transmit antenna elements (m_1 and m_2) can be expressed as [19]:

$$\rho_{n_1 n_2}^{R_x} = \left\langle |h_{mn1}|^2, |h_{mn2}|^2 \right\rangle \tag{7}$$

$$\rho_{m_1 m_2}^{T_x} = \left\langle |h_{nm1}|^2, |h_{nm2}|^2 \right\rangle \tag{8}$$

The general correlation expression between x and y is:

$$\langle x, y \rangle = \frac{E[xy] - E[x]E[y]}{\sqrt{\left(E\left[x^2\right] - E[x]^2\right)\left(E\left[y^2\right] - E[y]^2\right)}} \tag{9}$$

where $[\cdot]$ denotes the expected value operator. CDFs of computed correlation coefficients are shown in Fig. 8. The low correlation of BN-MIMO is due to its high ability for generating independent multipath, owing to its precise orthogonal radiation beams. Average "ρ" are summarized in Table 4. It is noteworthy mentioning that for a fixed channel gain, a higher K_{Factor} means an increase in the spatial correlation and hence a degradation in channel capacity [19]. However, this is not the case for BN-MIMO. Its high radiation gain results in strong multipath as compared to CMPA-MIMO. Under LOS, the inter-subchannels correlation coefficient reported in [2] is around 85%, obtained using two microstrip patch elements arrays (2×2 MIMO). Thus, the orthogonal radiation properties of both presented MIMO setups have been found to mitigate "ρ" considerably by about 23%, knowing that 4×4 MIMO generate a greater amount of independent multipath in the channel. Furthermore, the receiving side appears less correlated than the transmit side by about 3%, implying that more local scatters are present in the vicinity of Rx [21].

Table 4. Average transmit/receive inter-subchannels correlation coefficients and channel capacity for various scenarios.

Array Type:	CMPA		BN-MIMO	
Scenario:	LOS	NLOS	LOS	NLOS
Receive ρ^{Rx}	0.65	0.41	0.62	0.3
Transmit ρ^{Tx}	0.68	0.43	0.65	0.34
Capacity [bit/s/Hz]	7.75	11.58	8.81	15.93

3.4. Channel Capacity Performance

The channel capacity (C) expressed in bit/s/Hz depends not only on channel multipath but also on the total received power or, equivalently, the average SNR throughout the channel. These two factors are usually not independent [22]. Thus, during the analysis of MIMO capacity, it is an intuitive practice to normalize the channel H-matrices of each frequency realization before investigating the effects of SNR and multipath as parameters. The normalized channel matrix $\mathbf{H}_n$ for each channel realization is expressed as [23]:

$$\mathbf{H}_n = \mathbf{H}\sqrt{\frac{N_T N_R}{\|\mathbf{H}\|_F^2}} \quad \text{where} \quad \|\mathbf{H}\|_F = \sqrt{\sum_{i=1}^{N_T}\sum_{j=1}^{N_R}\left|H_{f(i,j)}^{MIMO}\right|^2} \tag{10}$$

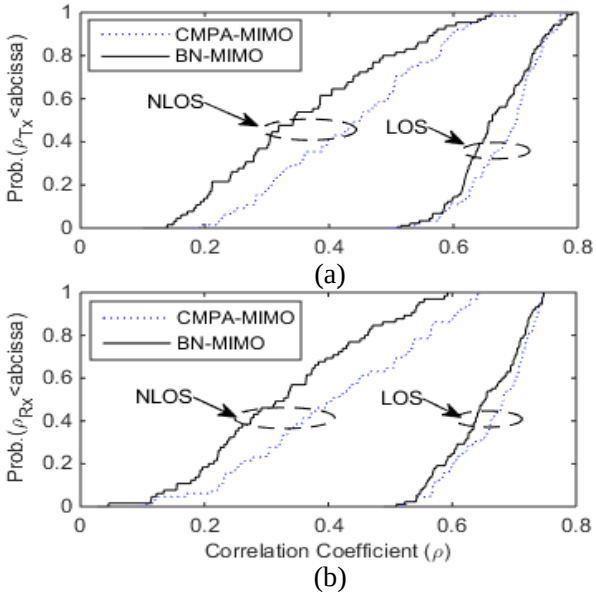

Figure 8. Cumulative distribution function (CDF) of the of correlation coefficients at (a) transmit side and (b) receive side.

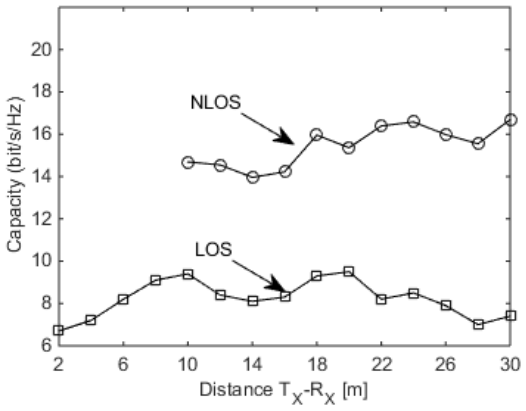

Figure 9. Channel capacity vs. T_X–R_X distance measured using BN-MIMO.

where $\|\mathbf{H}\|_F$ is the Frobenius coefficients matrix. Given the channel information at R_X, the channel capacity is expressed as [23]:

$$C = \log_2 \left\{ det \left[\mathbf{I}_{N_R} + \frac{\text{SNR}}{N_T} \mathbf{H}_n \mathbf{H}_n^* \right] \right\} \text{ bit/s/Hz} \tag{11}$$

where the superscript $(\cdot)^*$ denotes the Hermitian conjugate of the normalized channel matrix, and $\mathbf{I}$ is the identity matrix. Equation (10) gives insight into the logarithmic growth of MIMO systems capacity with respect to SNR assuming uncorrelated subchannels and that the channel state information (CSI) is perfectly known at the receiver. In order to evaluate the multipath effect on the channel capacity, an SNR of 10 dB is assumed in Equation (10) regardless of the position of the receiver throughout the gallery [5]. Results of Fig. 9 and Table 4 indicate that BN-MIMO yields an additional average capacity about 1.1 bit/s/Hz, 4.35 bit/s/Hz for LOS, NLOS cases, respectively, as compared to CMPA-MIMO.

Thus, no matter what the undertaken scenario is, the improvement in the link throughput speed in bit/s/Hz offered by BN-MIMO is noticeable. Compared to [5], the higher capacity performance of the presented BN-MIMO might be due to the following reasons: (i) a greater amount of multipath is

Table 5. BN array predominant performance over CMPA of [5].

Measurement Scenario		LOS	NLOS
Path Loss (PL)	suppression	2.2 dB	5.51 dB
PL gradient (n)	suppression	1.18 to 1.13	2.56 to 2.24
Signal-to-Noise Ratio (SNR)	Gain	4.2 dB	3.6 dB
Ricean K_{Factor}	Gain	1.6 dB	2.83 dB
RMS delay (σ_t)	suppression	0.67 ns	3.7 ns
Coherence Bandwidth (B_C)	Gain	4.6 MHz	0.82 MHz
Correlation Coefficient (ρ)			
Receiver ρ^{Rx}	suppression	4%	11%
Transmitter ρ^{Tx}	suppression	6%	9%
Capacity	Gain	1.1 bit/s/Hz	4.35 bit/s/Hz

present in the channel, and (ii) a lower inter-subchannels correlation results from the precise orthogonal radiation property of BN-MIMO.

Furthermore, under NLOS, BN-MIMO seems to offer almost twice the amount of the capacity over the linear planar microstrip patch arrays used in [5], which might be due to the above justifications.

4. CONCLUSION

Despite the heavy multipath of underground mine, the results reported in this experimental study confirm that the performance of MIMO systems in such environment does not depend on channel multipath only, but also on the radiation properties of the employed antenna arrays. Due to the high gain and orthogonal property of its radiation beams, BN-MIMO has shown an additional efficiency in gathering a greater amount of independent channel multipath as compared to CMPA-MIMO proposed in [5]. BN-MIMO offers a potential solution for enhancing the propagation characteristics as well as the spectral efficiency of underground mine channels. Table 5 shows the predomination of BN-MIMO over CMPAMIMO.

ACKNOWLEDGMENT

The authors gratefully acknowledge the financial support of National Sciences and Engineering council of Canada (NSERC) and the laboratory facilities provided by the LRTCS are also acknowledged.

REFERENCES

1. Yarkan, S., S. Guzelgoz, H. Arslan, and R. R. Murphy, "Underground mine communications: A survey," *IEEE Communications Surveys & Tutorials*, Vol. 11, No. 3, 125–142, 2009.
2. Rissafi, Y., L. Talbi, and M. Ghaddar, "Experimental characterization of an UWB propagation channel in underground mines," *IEEE Trans. Antennas and Propagation*, Vol. 60, No. 1, 240–246, Jan. 2012
3. Forooshani, A., S. Bashir, D. Michelson, and S. Noghanian, "A survey of wireless communications and propagation modeling in underground mines," *IEEE Communications Surveys & Tutorials*, Vol. 15, No. 14, 1524–1545, Nov. 2013.
4. Molisch, A. F., *Wireless Communications*, 2nd Edition, Wiley, 2011.
5. Ghaddar, M., M. Nedil, I. B. Mabrouk, and L. Talbi, "Multiple-input multiple-output beam-space for high-speed wireless communication in underground mine," *IET Microwaves, Antennas & Propagation*, Vol. 9, No. 13, Oct. 2015.

6. Nedil, M., T. A. Denidni, and L. Talbi, "Novel butler matrix using CPW multilayer technology," *IEEE Transactions on Microwave Theory and Techniques*, Vol. 54, No. 1, 499–507, Jan. 2006.
7. Hansen, R. C., *Phased Array Antennas*, John Wiley and Sons, New York, 1997.
8. Berke, C., A. Yusuf, and R. Gabriel, "An 8×8 Butler matrix in 0.13-µm CMOS for 5-6-GHz multibeam applications," *IEEE Transaction on Microwave Theory and Techniques*, Vol. 59, No. 2, Feb. 2011.
9. Grau, A., J. Romeu, and F. De Flaviis, "On the diversity gain using a butler matrix in fading MIMO environments," *Wireless Communications and Applied Computational Electromagnetics International Conference*, 478–481, Apr. 2005.
10. Ben Mabrouk, I., L. Talbi, and M. Nedil, "Performance evaluation of a MIMO system in underground mine gallery," *IEEE Antennas and Wireless Propagation Letters*, Vol. 11, 830–833, 2012.
11. Durgin, G., T. S. Rappaport, and H. Xu, "Measurements and models for radio path loss and penetration loss in and around homes and trees at 5.85 GHz" *IEEE Transactions on Communications*, Vol. 46, No. 11, 1484–1496, Nov. 1998.
12. Forooshani, A., R. White, and G. Michelson, "Effect of antenna array properties on multiple-input-multiple-output system performance in an underground mine" *IET Microwaves Antennas & Propagation*, Vol. 7, No. 13, 1035–8725, 2013.
13. Boutin, M., A. Benzakour, C. Despins, and E. Affés, "Radio wave characterization and modeling in underground mine tunnels" *IEEE Transactions on Antennas and Propagation*, Vol. 4, No. 5, 540–549, 2008.
14. Kang, M. and M. Alouini, "Capacity of MIMO Rician channels," *IEEE Transactions on Wireless Communications*, Vol. 5, No. 1, 112–122, 2006.
15. Rappaport, T. S., *Wireless Communications: Principle and Practice*, 2nd edition, Prentice Hall, PTR, NJ, USA, 2002.
16. Wang, Y., W. Lu, and H. Zhu, "Propagation characteristics of the LTE indoor radio channel with persons at 2.6 GHz," *IEEE Antennas and Propagation Letters*, Vol. 12, 991–994, 2013.
17. Ruisi, H., Z. Zhangdui, A. Bo, G. Ke, C. Binghao, J. AIonso, and C. Briso, "Propagation channel measurements and analysis at 2.4 GHz in subway tunnels," *IET Microwaves, Antennas and Propagation*, Vol. 7, No. 11, 934–941, 2013.
18. Molisch, A. F., *Wireless Communications*, 2nd edition, Wiley, 2011.
19. Cho, Y., J. Kim, W. Yang, and C. Kang, *MIMO-OFDM Wireless Communications with MATLAB*, John Wiley & Sons, 2010.
20. Ben Mabrouk, I., L. Talbi, and M. Nedil, "Performance evaluation of a MIMO system in underground mine gallery," *IEEE Antennas and Wireless Propagation Letters*, Vol. 11, 830–833, 2012.
21. Malik, W. Q., "Spatial correlation in ultrawideband channels," *IEEE Transactions on Wireless Communications*, Vol. 7, No. 2, 60–610, Feb. 2008.
22. Telatar, I. E., "Capacity of multi-antenna Gaussian channels," *AT&T Bell Lab Internal Tech. Memo.*, Oct. 1995.
23. Foschini, G. J. and M. J. Gans, "On limits of wireless communications in a fading environment when using multiple antennas," *Wireless Personal Communications*, Vol. 6, No. 3, 31–335, 1998.